Journal of Geodynamics 66 (2013) 53–58

Contents lists available at SciVerse ScienceDirect

Journal of Geodynamics

journal homepage: http://www.elsevier.com/locate/jog

Interseismic strain accumulation across the North Tabriz Fault (NW Iran) deduced from InSAR time series

Sadra Karimzadeh[a,*], Ziyadin Cakir[b], Batuhan Osmanoğlu[c], Gina Schmalzle[d], Masakatsu Miyajima[a], Reza Amiraslanzadeh[a], Yahya Djamour[e]

[a] Faculty of Environmental Design, Kanazawa University, Japan
[b] Geology Department, Istanbul Technical University, Turkey
[c] Geophysical Institute, University of Alaska Fairbanks, USA
[d] Earth and Space Sciences, University of Washington, USA
[e] Geomatics College, National Cartographic Center (NCC), Iran

ARTICLE INFO

Article history:
Received 27 August 2012
Received in revised form 15 January 2013
Accepted 3 February 2013
Available online xxx

Keywords:
North Tabriz Fault
InSAR
Slip rate
Subsidence
Interseismic strain accumulation

ABSTRACT

We present the surface deformation along the North Tabriz Fault (NTF) deduced from Synthetic Aperture Radar Interferometry (InSAR) technique. The NTF, a major right-lateral strike-slip fault within the active Arabia–Eurasia collision zone, is located 40–45 km southwest of the Mw 6.5 and Mw 6.3, August 11, 2012 earthquake sequence that caused heavy damage and more than 300 deaths in Ahar, NW Iran. InSAR time series analysis of 17 ENVISAT radar images acquired between 2004 and 2010 using combination of the permanent scatterers InSAR (PSI) and the small baseline InSAR (SBAS) approach reveals sub-centimeter interseismic strain accumulation across the NTF and rapid subsidence in the Tabriz basin. Elastic dislocation modeling of the mean line-of-sight velocity field estimated from SBAS time series yields an average slip rate of 8.7 ± 2.5 mm/year with a locking depth of 15.8 ± 10.8 km. This rate is consistent with previous geodetic estimates based on recent Global Positioning System measurements, and suggests a recurrence interval of 250–300 years for major earthquakes of Mw 7.0–7.3 on the NTF, much shorter than those estimated from paleoseismic investigations (821 ± 176 years). This in turn implies a high seismic potential on the NTF taking into account the occurrence of the two last earthquakes on the NTF in 1721 and 1780. SAR time series analysis also reveals three regions of rapid subsidence with a maximum rate of 20 mm/year near the Tabriz thermal power plant in the Tabriz basin. Piezometric data from groundwater wells suggest that accelerated subsidence over the last several years may result from fluctuations in the ground water table.

1. Introduction

Interaction of Arabian and Eurasian plates created prominent tectonic features in western Iran and eastern Turkey (Jackson, 1992). One major structure is the North Tabriz Fault (NTF) encompassed in a region of intense deformation and seismicity located between two fold-and-thrust belts of the Caucasus to the north and the Zagros Mountains to the south, spanning a length of 150 km in NW-SE direction in NW Iran (Berberian and Arshadi, 1976; Jackson, 1992; Fig. 1). The NTF is located ~40–45 km south-southwest of the Ahar region struck by the Mw 6.5 and Mw 6.3 earthquake sequence in August 11, 2012 (Fig. 2). Field observations conducted by Geological Survey of Iran show oblique right-lateral strike-slip surface faulting on a WNW-ESE trending rupture, consistent with focal mechanism solutions.

Geodetic and paleoseismic studies yield conflicting estimates of shear strain across the NTF (Djamour et al., 2011; Hessami et al., 2003a). While slip rate estimates based on offset streams and displaced historical structures such as traditional water channels (qanats) and other water pipelines yield 2–4 mm/year right-lateral horizontal movement across the NTF (Hessami et al., 2003a; Karakhanian et al., 2004), GPS measurements suggest much higher slip rates reaching 7–10 mm/year (Djamour et al., 2011; Masson et al., 2006; Reilinger et al., 2006; Vernant et al., 2004). Fault locking depths could not be estimated with a high level of accuracy due to sparse distribution of the GPS vectors around the NTF and their relatively higher errors due to limited (<4) number of measurements on some campaign sites (Djamour et al., 2011; Masson et al., 2006). The average distance between GPS stations is about 50 km (Djamour et al., 2011).

In this study, we use a multi temporal Synthetic Aperture Radar Interferometry technique (MT-InSAR) with the small baseline

* Corresponding author. Tel.: +81 8042579198.
E-mail addresses: s.karimzadeh@stu.kanazawa-u.ac.jp, sadra.karimzadeh@gmail.com (S. Karimzadeh).

0264-3707/$ – see front matter © 2013 Elsevier Ltd. All rights reserved.
http://dx.doi.org/10.1016/j.jog.2013.02.003

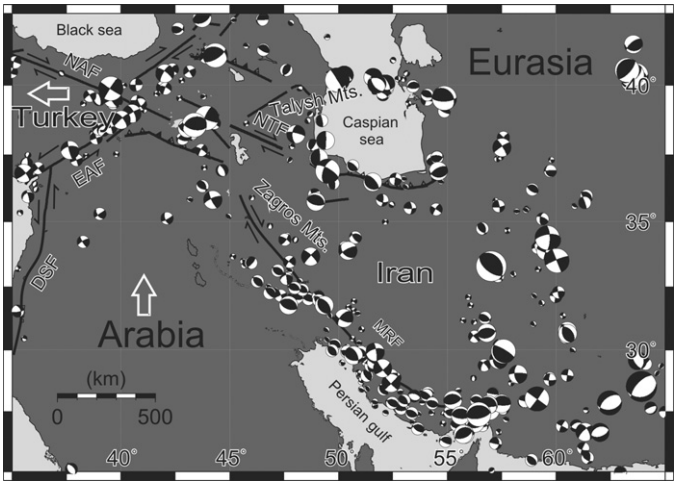

Fig. 1. Seismotectonic map of the study region. NTF, North Tabriz Fault; NAF, North Anatolian Fault; EAF, East Anatolian Fault; DSF, Dead Sea Fault; MRF, Main Recent Fault. Simplified major faults (black lines) around the Arabian–Eurasian collision zone with focal mechanisms of major earthquakes between 1976 and 2012 from the Global CMT (http://www.globalcmt.org/). White arrows sketch the motion of Arabian and Anatolian plate relative to Eurasia.

InSAR (SBAS) approach to map the velocity field around the Tabriz basin and central section of the NTF using ENVISAT Advanced SAR (ASAR) data acquired between 2003 and 2010 (Figs. 2 and 3). Unlike most of the studied faults elsewhere in the world (Elliott et al., 2008; Fialko, 2006; Wright et al., 2001), the low interseismic strain accumulation rate along the NTF is challenging for InSAR studies. However, like the eastern section of the North Anatolian Fault, the NTF with its NW-SE strike is optimally oriented for the ENVISAT imaging geometry since it lies almost parallel to the range direction, allowing for the detection of maximum fault-parallel horizontal motion that the radar can capture (Wright et al., 2001).

The study area is also ideal for the InSAR technique owing to its arid to semi arid climate and thus its sparse vegetation cover. We model the InSAR data to deduce the slip rate and locking depth of the NTF using an elastic dislocation model, and present evidence for land subsidence in the Tabriz basin, a large intramountain basin bounded by Lake Urmia to the west and the NTF to the

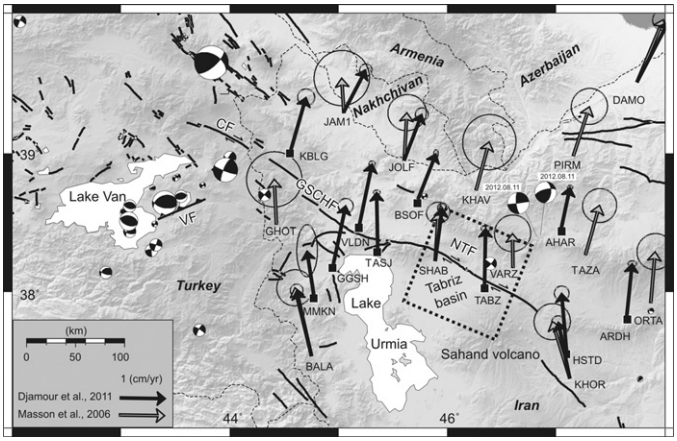

Fig. 2. Morphotectonic map of the study area within the Turkish–Iranian plateau showing active faults (black lines), focal mechanisms and GPS velocity fields relative to Eurasia with 95% confidence ellipses (with 4 letter site names) on shaded relief from SRTM-3 arc second data. Continuous GPS stations are indicated with black squares at vector tails. Black dashed square shows the frame of the SAR images studied, covering major part of the Tabriz basin and the NTF. GSCHF, Gailatu-Siah Chesmeh-Khoy Fault; VF, Van Fault (2012 Van rupture); CF, Chalderan Fault; NTF, North Tabriz Fault.

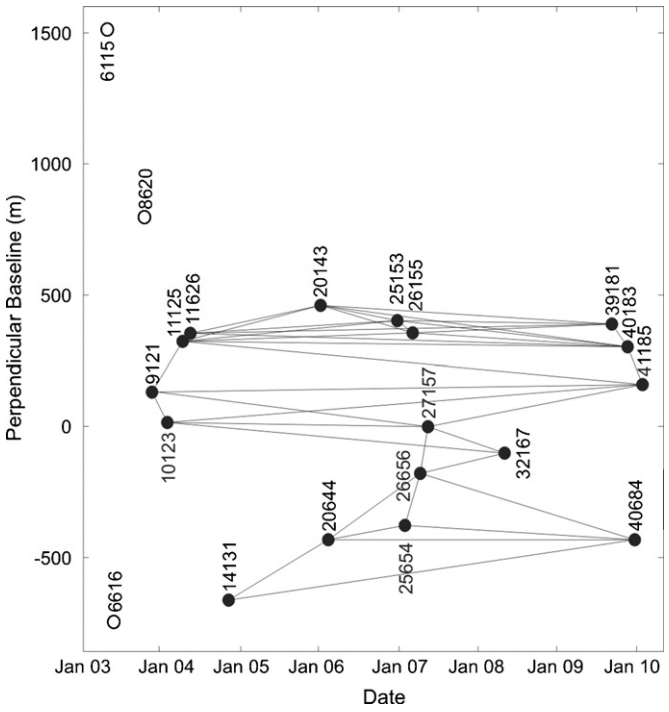

Fig. 3. Temporal (up to 7 years) and spatial (up to 400 m) baselines for the ENVISAT ASAR interferograms (lines) and orbit numbers analyzed between November 2004 and January 2010. Note that three scenes (open circles) are not used in the time series analysis as they fail to provide adequate coherence.

east-northeast between the Zagros and Talysh mountains (Figs. 1 and 2). The Tabriz basin hosts some important industrial structures, such as a thermal power plant, a petrochemical site and the Tabriz-Miandoab water lifeline, which may be threatened by the subsidence.

2. Seismotectonic setting

The study area is located on the Turkish–Iranian plateau where ongoing Arabian–Eurasian convergence is partitioned between thrusts and strike-slip faults in NW Iran and eastern Turkey (Copley and Jackson, 2006; Jackson, 1992; Fig. 1). The NTF is a right-lateral strike-slip fault that accommodates part of the convergence and forms the northern boundary of the Tabriz basin (TB) with a clear surface expression on the topography (Karakhanian et al., 2004). It is the southeastern continuation of the Gailatu-Siah Chesmeh-Khoy and Chalderan (Çaldıran in Turkish) faults that ruptured in 1976 with a Mw 7.1 earthquake in Turkey near the Iranian border (Toksoz et al., 1977; Fig. 2). Although discontinuous, this right-lateral system of strike-slip faults appears to be the southeastern continuation of the North Anatolian Fault into NW Iran (Djamour et al., 2011; Jackson, 1992; Westaway, 1990). Historical documents going back two millennia (Berberian and Arshadi, 1976) and instrumental records demonstrate that NW Iran and Eastern Turkey have been struck by numerous destructive earthquakes, the most recent largest one being the Mw 7.1, October 23, 2011 Van earthquake associated with reverse slip on a NE-SW trending fault (Akoglu et al., 2012; Fig. 2). Historical documents suggest that the last two large earthquakes on the NTF took place within 60 years in the 18th century on its adjacent segments (Ambraseys and Melville, 1982; Berberian and Arshadi, 1976). The first event occurred in 1721 and had a magnitude of Ms 7.3. Initiating at 37.90°N, 46.70°E (Berberian, 1994), it ruptured to the southeast along the NTF more than 39 km. The second earthquake in 1780 (Ms 7.4) broke its northwestern section with an epicenter located

at 38.12°N, 46.29°E and producing a surface rupture of ~100 km long (Ambraseys and Melville, 1982; Berberian, 1994). Although the direction and termination of these ruptures are not well known, the epicenters of the events and studies by Karakhanian et al. (2004) suggest that the SAR images analyzed in this study cover most of the 1780 rupture and possibly some sections of the 1721 event (Fig. 2). Therefore, the southern segment of the NTF, in particular, poses relatively higher seismic hazard, as it has not produced any large earthquake for nearly three centuries. A future earthquake on any of the two rupture segments would have a large impact for Tabriz as suggested by the historical documents reporting similar damages for the two events (Berberian, 1994).

3. Surface deformation field from InSAR

The InSAR technique combines radar images of the same region acquired at different times (i.e., repeat pass interferometry) or simultaneously but from a different angle of view (i.e., single pass interferometry) to obtain the interferometric phase, which gives a measure of the radar-to-ground range difference between the two images (Gabriel et al., 1989). While single pass interferometry is mostly used for constructing digital elevation models (DEM) (i.e., Shuttle Radar Topographic Mission (SRTM)), repeat pass interferometry is generally used for detecting surface movements. Details of the InSAR technique can be found in several review articles such as Massonnet and Fiegl (1998) and Bürgmann et al. (2000). Extracting surface deformation that occurred during the time interval covered by the two images in line of sight (LOS) direction requires removal of the phase contributed by topography and orbital separation, which can be done using DEMs and accurate estimates of the state vector of the satellite. Since its application to the 1992 Landers earthquake (Massonnet et al., 1993), the technique with its wide spatial coverage and high accuracy (sub cm), has been widely used to study crustal deformation due to the earthquake cycle (i.e., coseismic, postseismic and interseismic) (Bürgmann et al., 2000; Cakir et al., 2012; Wright et al., 2001) along numerous active faults of the world during the last two decades. The main limitation to the accuracy of InSAR measurements is due to atmospheric artifacts, DEM errors, orbital residual and poor coherence (Zebker et al., 1997). To minimize these errors, a relatively new and advanced technique, i.e., Multi temporal InSAR technique has been developed. This technique uses multi-temporal stacks of SAR images to generate time series of ground deformations for individual targets, named as Permanent Scatterers (PS) and small baseline InSAR (SBAS) (Berardino et al., 2002; Ferretti et al., 2001). Currently, there are two broad categories of multi temporal InSAR techniques (Sousa et al., 2011); (1) PS methods including those that use coherence estimation based on a temporal model of deformation (Ferretti et al., 2001) and those based on spatial correlation (Hooper, 2008), and (2) small baseline (SBAS) methods (Berardino et al., 2002; Schmidt and Bürgmann, 2003). Studies show that multi temporal InSAR techniques can resolve surface displacement of individual features at a level of about 0.5 mm/year using all data collected over the target area by a SAR satellite.

To investigate the surface motions in the Tabriz basin and its surroundings, we used in this study the Stanford Method for PS technique (StaMPS) that uses both PS and SBAS InSAR techniques (Hooper et al., 2004, 2007; Hooper, 2008; Sousa et al., 2011). The most recent version of StaMPS (StaMPS/MTI) can also combine both sets of results (PS and SBAS) to improve phase unwrapping and the spatial sampling of the signal of interest (Sousa et al., 2011). This technique recognizes potential persistent scatterer candidates using amplitude dispersion index (ADI). In addition to persistent scatterers, StaMPS also detects and uses slowly decorrelating filtered phase pixels (SDFP). The number of stable points (SP = PS + SDFP) candidates increases with increasing ADI. Number of persistent scatterer candidates has a significant role in detecting interseismic movements. However, there is a tradeoff between number of persistent scatterer candidates and number of unreliable targets as larger ADI values result in more unreliable points. Generally persistent scatterers density varies with terrain (i.e., 0–10 persistent scatterers/km^2 in mountainous areas and about 100 persistent scatterers/km^2 for urban areas). In our processing we use 0.42 for ADI and divide the scene in 5 × 5 patches with 200 and 1000 overlapping pixels (~4 km.) in the range and azimuth directions, respectively. Large overlaps between the patches ensure reliable merging of them at later stages of processing. In this study, we use a SBAS style network minimizing the perpendicular, temporal and Doppler baselines to maximize the correlation of generated interferograms and increasing the number of observable ground points. Unlike the SBAS approach described by Berardino et al. (2002), StaMPS uses the full resolution (i.e., SLC) images instead of multi-looked scenes.

Interferograms from 20 ASAR single look complex (SLC) images of the European Space Agency's (ESA) ENVISAT satellite were processed with relatively short spatial (<400 m) and temporal (7 years) baselines using the DORIS InSAR processing software (Kampes and Usai, 1999). Topographic phase was removed using the ASTER digital elevation model (30-m posting) and ESA's precise DORIS orbits (DOR_VOR_AX). The images cover an area of ~100 km × 100 km and were acquired from the descending orbit on track 392 in I2 swath mode (23° look angle in the image center) between May 2003 and January 2010 (Fig. 2). As shown in Fig. 3, interferograms from some orbits (i.e., 6115, 6616 and 8620) could not be used due to their long temporal and perpendicular baselines.

Fig. 4 shows the mean LOS velocity field obtained from SBAS time series using 39 interferograms corrected for DEM errors using the v-d option in StaMPS. Owing to the arid to semi-arid climate of the region an abundant number of SP (>110,000) are found in the rural areas as well as the urban sites. To eliminate orbital residuals, a best-fitting least-squares plane is removed from the LOS velocity field using the SP on the gentle slopes of Sahand volcano east of the Tabriz basin and south of the NTF to avoid regions of land subsidence in the alluvial plane, shear strain in the near field, and potential atmospheric effects correlated with rugged high topography to the north. The most prominent feature in the LOS velocity field is the circular regions with yellow-to-red color where the fastest surface displacements occur between 2003 and 2010. Their circular pattern indicates rapid subsidence of up to 20 mm/year is restricted mainly to the Quaternary fine-grained alluvial plane of the Tabriz basin close to the Tabriz thermal power plant (Fig. 5). SBAS time series show that subsidence has occurred over the last few years (Fig. 6). Piezometer measurements suggest the subsidence in the Tabriz basin may result from large seasonal fluctuations in the groundwater table since 2008 while Razzaghmanesh et al. (2006) attributes the general subsidence in the Tabriz basin to excessive groundwater extraction that reaches 5 million cubic meters per year, nearly twice of the yearly charge of the aquifer.

Surface change due to the tectonic motion is detected in the LOS velocity field (Fig. 4). While the color contrast in LOS velocity between the southern (mostly green) and northern (mostly blue) sides of the NTF reveals the differential motion between the two blocks, the gradual color change across the fault attests to the interseismic strain accumulation. Therefore, the SAR data can be used in estimating the locking depth and slip rate of the NTF.

4. Modeling the strain accumulation across the North Tabriz Fault

Modeling of the InSAR data is carried out using screw dislocations for an infinitely long vertical fault in an elastic half space (Cakir

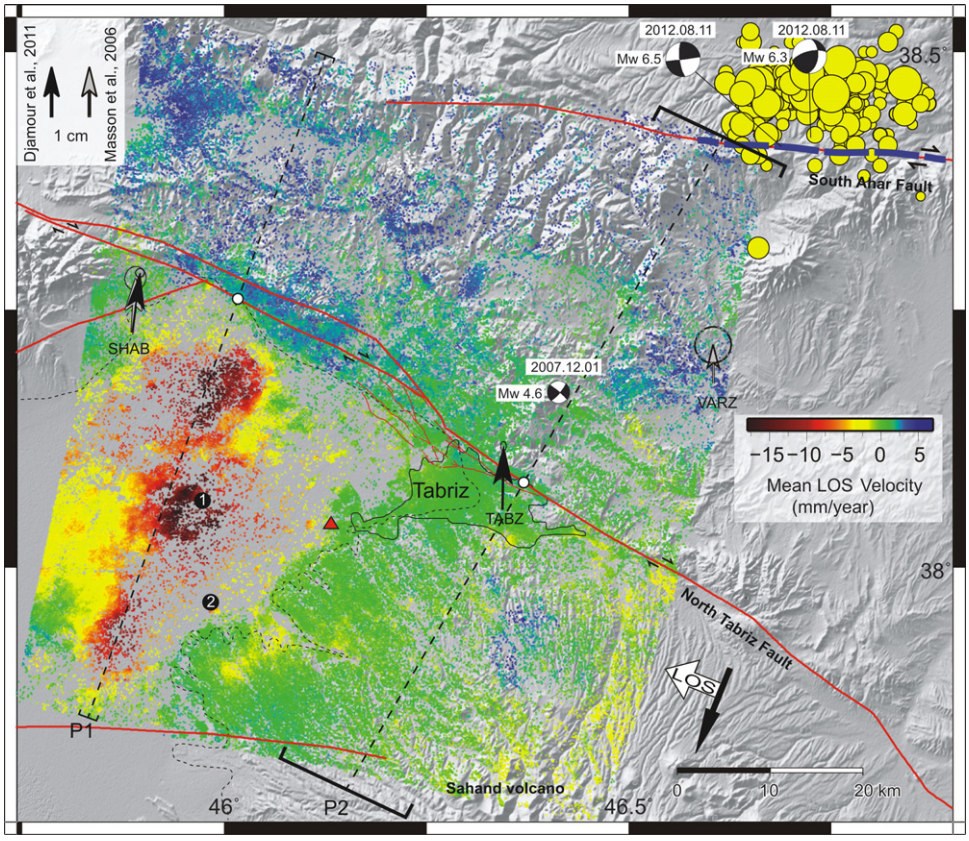

Fig. 4. Color-coded mean LOS velocity field between 2003 and 2010 in the Tabriz region plotted on SRTM shaded relief image with GPS vectors, locations of wells (numbered black circles) and active faults (red lines; from Hessami et al., 2003b and Karakhanian et al., 2004). Movements away from the satellite are shown with warm colors and toward the satellite are cool colors. Combined white and black arrows indicate satellite's LOS look and flight directions, respectively. Thick dashed lines are profiles with white circles indicating the origin of horizontal axes of plots shown in Figs. 5 and 7. Brackets show the sampling width for InSAR data. Polygons with dashed and solid lines mark the boundaries of Quaternary alluvial sediments and Tabriz city, respectively. Red triangle shows the location of Tabriz Power Plant. Yellow circles and dashed blue line show distribution of aftershocks and surface rupture of the Mw 6.5 and Mw 6.3, August 11, 2012 Ahar earthquake sequence, respectively. Focal mechanisms are from Global CMT catalog.

et al., 2012; Motagh et al., 2007; Savage and Burford, 1973; Segall, 2002; Tatar et al., 2012). The locking depth, slip rate and shift in reference point velocity are estimated within 95% confidence limits using a Levenberg–Marquart nonlinear optimization algorithm with no a priori bounds. The fault position is defined by the surface trace of the NTF (Karakhanian et al., 2004) and is kept fixed during the inversion (white circles in Fig. 4). The mean LOS velocity field is converted to fault parallel mean InSAR velocities field assuming that the LOS range changes are due to purely horizontal motion on the NTF (Lyons and Sandwell, 2003). In modeling, we used data within a 15 km wide fault-perpendicular profile across the NTF east of the SAR image frame, away from the Tabriz basin where rapid surface subsidence is dominant (Fig. 4). A mean SBAS velocity and its standard deviation are calculated at every km along the profile as shown in Fig. 7 with the fault parallel component of the GPS vectors within a distance of 100 km on each side of the NTF. Although noisy, the mean SBAS velocity change across the fault reveals the typical arctangent pattern of interseismic strain accumulation for strike-slip faults (Motagh et al., 2007; Wright et al., 2001). Absence of correlation between the mean fault parallel velocities and topography along the profiles suggests that tropospheric artifacts are

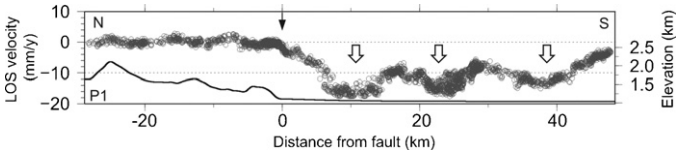

Fig. 5. LOS velocity profile P1 across showing the three main subsiding regions (indicated with white arrows) in the Tabriz basin (see Fig. 4 for its location). Black arrow indicates the location of the North Tabriz Fault where the profile begins. Topography along the profile shown with a black line does not show a clear correlation with LOS velocity.

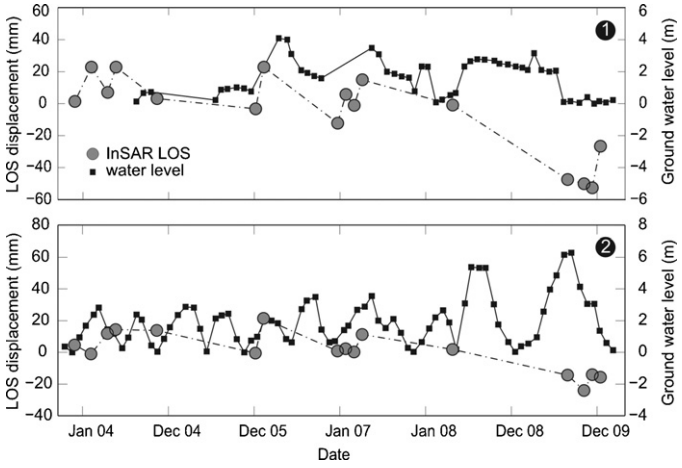

Fig. 6. Time series of InSAR data and groundwater table measurements in the Tabriz basin (see Fig. 4 for location). The noise in InSAR time series is most probably due to atmospheric artifacts. Although not very high, correlation of the two measurements suggests that the subsidence in the Tabriz basin probably result from large seasonal fluctuations in the groundwater table that occurred mostly over the last few years.

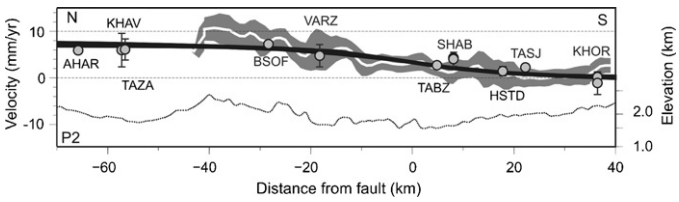

Fig. 7. Modeling of InSAR measurements. Mean InSAR (white line enveloped by 1 sigma error band) and GPS (gray circles with vertical error bars showing 95% confidence interval) fault-parallel horizontal velocities along profile P2 shown in Fig. 4. Thick black curve is the best fitting elastic dislocation model with a line thickness showing 95% prediction bounds. Topographic profiles (dotted lines) are shown in order to reveal any potential correlation between topography and InSAR measurements.

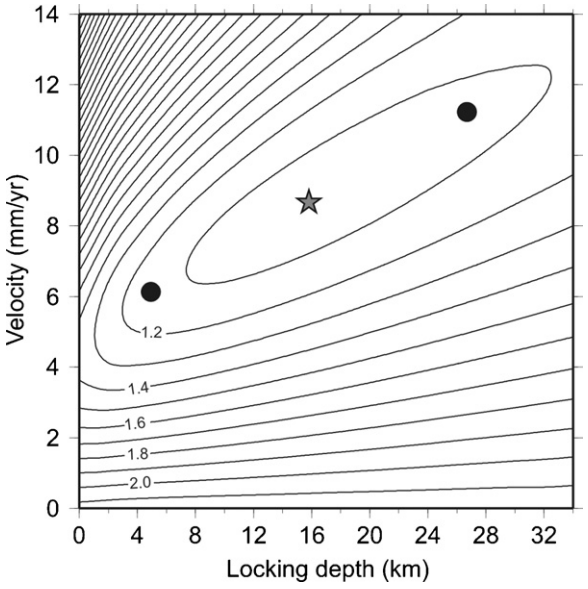

Fig. 8. Contour map of RMS misfit (mm) between InSAR and GPS observations in Fig. 7 and models with varying locking depths and slip rates. The trade off between the two parameters is evident. Star indicates the best misfit model parameters plotted in Fig. 7. Black circles show upper and lower bounds of 95% confidence interval.

negligible. Joint inversion of the SBAS (88 points) and the GPS (11 points) data (Djamour et al., 2011; Masson et al., 2006) weighted by the uncertainty in each GPS data point and standard deviation of SBAS data yields a slip rate of 8.7 ± 2.5 mm/year for the NTF, in good agreement with previously estimated slip rates of 7–10 mm/year from GPS measurements (Djamour et al., 2011; Masson et al., 2006; Reilinger et al., 2006; Vernant et al., 2004). As illustrated in Fig. 8, the locking depth is poorly constrained and is 15.8 ± 10.8 km, similar to the estimates of Djamour et al. (2011) that range between 6 and 26 km.

5. Discussions and conclusion

The rate at which a fault slips determines the seismic hazard that it represents because average earthquake recurrence intervals tend to decrease as slip rates increase (Roberts et al., 2004). Thus, higher geodetic slip rates imply shorter recurrence interval for large earthquakes on the NTF as opposed to those determined by paleoseismic studies based on trenching (Hessami et al., 2003a). Therefore, estimating the rate of interseismic strain accumulation across the NTF is critical in determining earthquake potential and seismic hazard for the city of Tabriz, the fourth most populous city in Iran with a population of over 1.5 million.

Hence, we used a multi temporal InSAR technique to deduce the slip of the North Tabriz Fault using 17 ENVISAT ASAR images acquired during a period of 6 years between 2004 and 2010. Elastic dislocation modeling of the InSAR data yields an average slip rate of 8.7 ± 2.5 mm/year, in agreement with previous geodetic estimates based on recent GPS measurements. This supports the inference of Djamour et al. (2011) that earthquake recurrence intervals for large earthquake (Mw 7–7.3) on the NTF are about 250–300 years, much shorter than that (821 ± 176 years) estimated by Hessami et al. (2003a) with paleoseismic investigations (see Wells and Coppersmith (1994) for the empirical relationship between average coseismic slip and magnitude for strike slip earthquakes). Therefore, an elapse time of 232 and 291 years since the two last major earthquakes nearby Tabriz on the NTF implies a high potential for a large earthquake in the next several decades.

This study demonstrates once again that interseismic strain accumulation with a sub-centimeter rate can be successfully detected and measured by multi temporal InSAR techniques (Gourmelen et al., 2011) in arid to semi arid regions. Therefore, SBAS or similar time series techniques can be applied to other sections of this fault system in Turkey and Iran.

Land subsidence is one of the major environmental problems in Iran (Dehghani et al., 2009; Motagh et al., 2008) and elsewhere in the world (Osmanoğlu et al., 2011). Piezometric data from groundwater wells collected by the Regional Water Organization, used for cooling the Tabriz thermal power plant and agricultural purposes suggest that large fluctuations occur in the ground water table, which may cause compaction of fine-grained sediments and thus subsidence on the surface (Fig. 6). Progressive subsidence south of the Tabriz basin near Lake Urmia, as well as declining water levels at this lake, is thought (Kabiri et al., 2012; Moghtased-Azar et al., 2012) to be due to climate change, local dams and excessive water removal. The current subsidence rates of up to 20 mm/year may threaten urban and industrial infrastructure if it expands toward Tabriz. Therefore, monitoring the land subsidence is critical for natural hazard assessments in this region.

Acknowledgments

We thank European Space Agency for providing ENVISAT ASAR data through the project CAT-1-8094. Two anonymous reviewers helped us improve and clarify very much the presentation of the manuscript. We have also benefited from our discussions with Dr. Fallahi. We also thank the Editor-in-Chief, R. Stephenson, for handling the manuscript. Most figures were generated using the public license Generic Mapping Tools software (Wessel and Smith, 1995). Ziyadin Cakir's contribution is partially supported by TUBITAK project 107Y281. This work is supported by Kanazawa University, Japan.

References

Akoglu, A.M., Jonsson, S., Cakir, Z., Ergintav, S., Dogan, U., Feng, G., Zabcı, C., 2012. The Surface Deformation and Source Parameters of the October 23rd, 2011, Mw 7.1 Van (Turkey) Earthquake from InSAR, GPS and Field Observations. EGU General Assembly, Vienna, Austria.

Ambraseys, N.N., Melville, C.P., 1982. A History of Persian Earthquakes. Cambridge University Press, New York.

Berardino, P., Fornaro, G., Lanari, R., Sansosti, E., 2002. A new algorithm for surface deformation monitoring based on small baseline differential SAR interferograms. IEEE Transactions on Geoscience and Remote Sensing 245 (40), 2375–2383.

Berberian, M., 1994. Natural hazards and the first earthquake catalogue of Iran. International Institute of Earthquake Engineering and Seismology 1, 266–270.

Berberian, M., Arshadi, S., 1976. On the evidence of the youngest activity of the North Tabriz Fault and the seismicity of Tabriz city. Geological Survey of Iran 39, 397–418.

Bürgmann, R., Rosen, P., Fielding, E., 2000. Synthetic aperture radar interferometry to measure Earth's surface topography and its deformation. Annual Review of Earth and Planetary Sciences 28, 169–209.

Cakir, Z., Ergintav, S., Ozener, H., Dogan, U., Akoglu, A., Meghraoui, M., Reilinger, R., 2012. Onset of aseismic creep on major strike slip faults. Geology 40 (12), 1115–1118.

Copley, A., Jackson, J., 2006. Active tectonics of the Turkish–Iranian Plateau. Tectonics 25, TC6006.

Dehghani, M., ValadanZoej, M.J., Entezam, I., Mansourian, A., Saatchi, S., 2009. InSAR monitoring of progressive land subsidence in Neyshabour, Northeast Iran. Geophysical Journal International 178, 47–56.

Djamour, Y., Vernant, P., Nankali, H.R., Tavakoli, F., 2011. NW Iran-eastern Turkey present-day kinematics: results from the Iranian permanent GPS network. Earth and Planetary Science Letters 307, 27–34, http://dx.doi.org/10.1016/j.epsl.2011.04.029.

Elliott, J.R., Biggs, J., Parsons, B., Wright, T.J., 2008. InSAR slip rate determination on the Altyn Tagh Fault, northern Tibet, in the presence of topographically correlated atmospheric delays. Geophysical Research Letters 35, L12309.

Ferretti, A., Prati, C., Rocca, F., 2001. Permanent scatters in SAR interferometry. IEEE Transactions on Geoscience and Remote Sensing 39 (1), 8–20.

Fialko, Y., 2006. Interseismic strain accumulation and the earthquake potential on the southern San Andreas fault system. Nature 441, 968–971.

Gabriel, A.K., Goldstein, R.M., Zebker, H.A., 1989. Mapping small elevation changes over large areas: differential radar interferometry. Journal of Geophysical Research 94, 9183–9191, B7.

Gourmelen, N., Dixon, T.H., Amelung, F., Schmalzle, G., 2011. Acceleration and evolution of faults: an example from the Hunter Mountain–Panamint Valley fault zone, Eastern California. Earth and Planetary Science Letters, 337–344, http://dx.doi.org/10.1016/j.epsl.2010.11.016.

Hessami, K., Pantosi, D., Tabassi, H., Shabanian, E., Abbassi, M., Feghhi, K., Solaymani, S., 2003a. Paleoearthquakes and slip rates of the North Tabriz Fault, NW Iran: preliminary results. Annales Geophysicae 46, 903–915.

Hessami, K., Jamali, F., Tabassi, H., 2003. Major active faults of Iran: Tehran, Iran, International Institute of Earthquake Engineering and Seismology, 1 sheet, scale 1:2,500,000.

Hooper, A., Zebker, H., Segall, P., Kampes, B., 2004. A new method for measuring deformation on volcanoes and other natural terrains using InSAR persistent scatterers. Geophysical Research Letters 31, L23611.

Hooper, A., Segall, P., Zebker, H., 2007. Persistent scatterer InSAR for crustal deformation analysis, with application to Volcán Alcedo, Galápagos. Journal of Geophysical Research 112, B07407, http://dx.doi.org/10.1029/2006JB004763.

Hooper, A., 2008. A multi-temporal InSAR method incorporating both persistent scatterer and small baseline approaches. Geophysical Research Letters 35, L16302.

Jackson, J., 1992. Partitioning of strike-slip and convergent motion between Eurasia and Arabia in Eastern Turkey and the Caucasus. Journal of Geophysical Research 97 (B9), 12471–12479.

Karakhanian, A., Trifonov, G., Philip, H., Avagyan, A., Hessami, K., Jamali, F., Bayraktutan, M., Bagdassarian, H., Arakelian, S., Davtian, V., Adilkhanyan, A., 2004. Active faulting and natural hazards in Armenia, eastern Turkey and Northern Iran. Tectonophysics 380, 189–219, http://dx.doi.org/10.1016/j.tecto.2003.09.020

Kabiri, K., Pradhan, B., Sharifi, A., Ghobadi, Y., Pirasteh, S.,2012. Manifestation of remotely sensed data coupled with field measured meteorological data for an assessment of degradation of Urmia Lake, Iran, vol. 6. In: Asia Pacific Conference on Environmental Science and Technology. APEST, Kuala Lumpur, Malaysia.

Kampes, B., Usai, S., 1999. Doris: the delft object-oriented radar interferometric software. In: Proc. 2nd International Symposium Operationalization of Remote Sensing, http://citeseerx.ist.psu.edu/viewdoc/summary?doi=10.1.1.46.1689

Lyons, S., Sandwell, D., 2003. Fault-creep along the southern San Andreas from InSAR, permanent scatterers, and stacking. Journal of Geophysical Research 108 (2047), 24.

Masson, F., Djamour, Y., Van Gorp, S., Chery, J., Tatar, M., Tavakoli, F., Nankali, H., Vernant, P., 2006. Extension in NW Iran driven by the motion of the South Caspian Basin. Earth and Planetary Science Letters 252, 180–188, http://dx.doi.org/10.1016/j.epsl.2006.09.038.

Massonnet, D., Rossi, M., Carmona, C., Adragna, F., Peltzer, G., Feigl, K., Rte, T., 1993. The displacement field of the Landers earthquake mapped by radar interferometry. Nature 364, 138–142.

Massonnet, D., Fiegl, K.L., 1998. Radar interferometry and its application to changes in the earth's surface. Reviews of Geophysics 36 (4), 441–500.

Moghtased-Azar, K., Mirzaei, A., Nankali, H.R., Tavakoli, F., 2012. Investigation of correlation of the variations in land subsidence (detected by continuous GPS measurements) and methodological data in the surrounding areas of Lake Urmia. Nonlinear Processes in Geophysics 19, 675–683.

Motagh, M., Hoffmann, J., Kampes, B., Baes, M., Zschau, J., 2007. Strain accumulation across the Gazikoy–Saros segment of the North Anatolian Fault inferred from Persistent Scatterer Interferometry and GPS measurements. Earth and Planetary Science Letters 255, 432–444, http://dx.doi.org/10.1016/j.epsl.2007.01.003.

Motagh, M., Walter, T.R., Sharifi, M.A., Fielding, E., Schenk, A., Anderssohn, J., Zschau, J., 2008. Land subsidence in Iran caused by widespread water reservoir overexploitation. Geophysical Research Letters 35, L16403.

Osmanoğlu, B., Dixon, T.H., Wdowinski, S., Cabral-Cano, E., Jiang, Y., 2011. Mexico City subsidence observed with persistent scatterer InSAR. International Journal of Applied Earth Observation 13 (1), 1–12, http://dx.doi.org/10.1016/j.jag.2010.05.009.

Razzaghmanesh, M., Salemi, T., Seraj, M., 2006. Ground water quality and quantity of Tabriz plain. National Conference on Irrigation and Drainage Network Management (In Persian).

Reilinger, R., McClusky, S., Vernant, P., Lawrence, S., Ergintav, S., Cakmak, R., Ozener, H., Kadirov, F., Guliev, I., Stepanyan, R., Nadariya, M., Hahubia, G., Mahmoud, S., Sakr, K., ArRajehi, A., Paradissis, D., Al-Aydrus, A., Prilepin, M., Guseva, T., Evren, E., Dmitrotsa, A., Filikov, S.V., Gomez, F., Al-Ghazzi, R., Karam, G., 2006. GPS constraints on continental deformation in the Africa Arabia-Eurasia continental collision zone and implications for the dynamics of plate interactions. Journal of Geophysical Research 111, B05411.

Roberts, G.P., Cowie, P.A., Papanikolaou, I., Michetti, A.M., 2004. Fault scaling relationships, deformation rates and seismic hazards: an example from the Lazio–Abruzzo Apennines, central Italy. Journal of Structural Geology 26, 377–398, http://dx.doi.org/10.1016/S0191-8141(03)00104-4.

Savage, J., Burford, R., 1973. Geodetic determination of relative plate motion in Central California. Journal of Geophysical Research 78, 832–845.

Schmidt, D.A., Bürgmann, R., 2003. Time dependent land uplift and subsidence in the Santa Clara valley, California, from a large InSAR data set. Journal of Geophysical Research 108, http://dx.doi.org/10.1029/2002JB002267.

Segall, P., 2002. Integration of geologic and geodetic estimates of fault slip rates on the San Andreas system. International Geology Review 44, 62–82.

Sousa, J.J., Hooper, A.J., Hanssen, R.F., Bastos, L.C., Ruiz, A.M., 2011. Persistent scatterer InSAR: a comparison of methodologies based on a model of temporal deformation vs. spatial correlation selection criteria. Remote Sensing of Environment 115 (10), 2652–2663.

Tatar, O., Poyraz, F., Gursoy, H., Cakir, Z., Ergintav, S., Akpinar, Z., Kocbulut, F., Sezen, F., Türk, T., Hastaoglu, K.O., Polat, A., Mesci, B.L., Gursoy, O., Ayazlı, I.E., Cakmak, R., Belgen, A., Yavasoglu, H., 2012. Crustal deformation and kinematics of the Eastern Part of the North Anatolian Fault Zone (Turkey) from GPS measurements. Tectonophysics 518–521, 55–62, http://dx.doi.org/10.1016/j.tecto.2011.11.010.

Toksoz, M.N., Arpat, E., Saroglu, F., 1977. East Anatolia earthquake of 24 November, 1976. Nature 270, 423–425.

Vernant, P., Nilforoushan, F., Hatzfeld, D., Abbassi, M.R., Vigny, C., Masson, F., Nankali, H., Martinod, J., Ashtiani, A., Bayer, R., Tavakoli, F., Chery, J., 2004. Present-day crustal deformation and plate kinematics in the Middle East constrained by GPS measurements in Iran and northern Oman. Geophysical Journal International 157, 381–398.

Wells, D.L., Coppersmith, K.J., 1994. New empirical relationships among magnitude, rupture length, rupture width, rupture area, and surface displacement. Bulletin of the Seismological Society of America 84, 974–1002.

Wessel, P., Smith, W.H.F., 1995. New version of the generic mapping tools released. Eos, Transactions American Geophysical Union 33, 329.

Westaway, R., 1990. Block rotation in western Turkey 1. Observational evidence. Journal of Geophysical Research 95 (B12), 19857–19884.

Wright, T., Parsons, B., Fielding, E., 2001. Measurement of interseismic strain accumulation across the North Anatolian Fault by satellite radar interferometry. Geophysical Research Letters 28, 2117–2120.

Zebker, H.A., Rosen, P.A., Hensley, S., 1997. Atmospheric effects in interferometric synthetic aperture radar surface deformation and topographic maps. Journal of Geophysical Research 102 (2), 7547–7563.